Al 6 2 − — Fusion of Two Aromatic Al 3 − Units. A Combined Photoelectron Spectroscopy and ab Initio Study of M + [Al 6 2 −] (M = Li, Na, K, Cu, and Au)

ARTICLE *in* JOURNAL OF THE AMERICAN CHEMICAL SOCIETY · NOVEMBER 2002

Impact Factor: 12.11 · DOI: 10.1021/ja027423g · Source: PubMed

5 AUTHORS, INCLUDING:

Aleksey E. Kuznetsov
Universidade Federal de São Carlos
67 PUBLICATIONS **2,056** CITATIONS
SEE PROFILE

Alexander I Boldyrev
Utah State University
339 PUBLICATIONS **9,771** CITATIONS
SEE PROFILE

Lai-Sheng Wang
Brown University
407 PUBLICATIONS **17,294** CITATIONS
SEE PROFILE

J|A|C|S
ARTICLES
Published on Web 09/06/2002

Al_6^{2-} − Fusion of Two Aromatic Al_3^- Units. A Combined Photoelectron Spectroscopy and ab Initio Study of $M^+[Al_6^{2-}]$ (M = Li, Na, K, Cu, and Au)

Aleksey E. Kuznetsov,[†] Alexander I. Boldyrev,*[,†] Hua-Jin Zhai,[‡] Xi Li,[‡] and Lai-Sheng Wang*[,‡]

Contribution from the Department of Chemistry and Biochemistry, Utah State University, Logan, Utah 84322-0300, Department of Physics, Washington State University, 2710 University Drive, Richland, Washington 99352, and W. R. Wiley Environmental Molecular Sciences Laboratory, Pacific Northwest National Laboratory, MS K8-88, P.O. Box 999, Richland, Washington 99352

Received June 23, 2002

Abstract: Photoelectron spectroscopy is combined with ab initio calculations to elucidate the structure and chemical bonding of a series of MAl_6^- (M = Li, Na, K, Cu, and Au) bimetallic clusters. Well-resolved photoelectron spectra were obtained for MAl_6^- (M = Li, Na, Cu, and Au) at several photon energies. The ab initio calculations showed that all of the MAl_6^- clusters can be viewed as an M^+ cation interacting with an Al_6^{2-} dianion. Al_6^{2-} was found to possess an O_h ground-state structure, and all of the MAl_6^- clusters possess a C_{3v} ground-state structure derived from the O_h Al_6^{2-}. Careful comparison between the photoelectron spectral features and the ab initio one-electron detachment energies allows us to establish firmly the C_{3v} ground-state structures for the MAl_6^- clusters. A detailed molecular orbital (MO) analysis is conducted for Al_6^{2-} and compared with Al_3^-. It was shown that Al_6^{2-} can be considered as the fusion of two Al_3^- units. We further found that the preferred occupation of those MOs derived from the sums of the empty 2e′ MOs of Al_3^-, rather than those derived from the differences between the occupied $2a_1'$ and $2a_2''$ MOs of Al_3^-, provides the key bonding interactions for the fusion of the two Al_3^- into Al_6^{2-}. Because there are only four bonding MOs (one π and three σ MOs), an analysis of resonance structures was performed for the O_h Al_6^{2-}. It is shown that every face of the Al_6^{2-} octahedron still possesses both π- and σ-aromaticity, analogous to Al_3^-, and that in fact Al_6^{2-} can be viewed to possess three-dimensional π- and σ-aromaticity with a large resonance stabilization.

Introduction

Small Al-based clusters have become a rich area of research in cluster physics and chemistry. The relatively simple electronic structure of Al has allowed numerous experimental and theoretical efforts to tailor the geometrical and electronic structures of small Al-based clusters by doping heteroatoms[1−23] and to explore novel chemical bonding in these small clusters.[24] Among interesting recent developments, pentaatomic tetracoordinate planar carbon[25−29] and all-metal aromaticity (both σ- and

* To whom correspondence should be addressed. E-mail: (A.I.B.) boldyrev@cc.usu.edu; (L.-S.W.) ls.wang@pnl.gov.
[†] Utah State University.
[‡] Washington State University and Pacific Northwest National Laboratory.

(1) Gong, X. G.; Kumar, V. *Phys. Rev. Lett.* **1993**, *70*, 2078.
(2) Cheng, H. P.; Barnett, R. N.; Landman, U. *Phys. Rev. B* **1993**, *48*, 1820.
(3) Gong, X. G.; Kumar, V. *Phys. Rev. B* **1994**, *50*, 17701.
(4) Nakajima, A.; Kishi, T.; Sugioka, T.; Kaya, K. *Chem. Phys. Lett.* **1991**, *187*, 239.
(5) Khanna, S. N.; Jena, P. *Phys. Rev. B* **1995**, *51*, 13705.
(6) Menezes, W. J. C.; Knickelbein, M. B. *Chem. Phys. Lett.* **1991**, *183*, 357.
(7) Kumar, K.; Sundararajan, V. *Phys. Rev. B* **1998**, *57*, 4939.
(8) Nakajima, A.; Hoshino, K.; Sugioka, T.; Naganuma, T.; Taguwa, T.; Yamada, Y.; Watanabe, K.; Kaya, K. *J. Phys. Chem.* **1993**, *97*, 86.
(9) Krissinel, E. B.; Jellinek, J. *Chem. Phys. Lett.* **1997**, *272*, 301.
(10) Majumder, C.; Das, G. P.; Kulshrestha, S. K.; Shah, V.; Kanhere, D. G. *Chem. Phys. Lett.* **1996**, *261*, 515.
(11) Ashman, C.; Khanna, S. N.; Pederson, M. R.; Kortus, J. *Phys. Rev. B* **2000**, *62*, 16956.
(12) Rao, B. K.; Jena, P. *J. Chem. Phys.* **2000**, *113*, 1508.
(13) Rao, B. K.; Jena, P. *J. Chem. Phys.* **2001**, *115*, 778.
(14) Leskiw, B. D.; Castleman, A. W., Jr.; Ashman, C.; Khanna, S. N. *J. Chem. Phys.* **2001**, *114*, 1165.
(15) Thomas, O. C.; Zheng, W.-J.; Lippa, T. P.; Xu, S.-J.; Lyapustina, S. A.; Bowen, K. H., Jr. *J. Chem. Phys.* **2001**, *114*, 9895.
(16) Thomas, O. C.; Zheng, W.-J.; Bowen, K. H., Jr. *J. Chem. Phys.* **2001**, *114*, 5514.
(17) Khanna, S. N.; Ashman, C.; Rao, B. K.; Jena, P. *J. Chem. Phys.* **2001**, *114*, 9792.
(18) Zope, R. R.; Baruah, T. *Phys. Rev. A* **2001**, *64*, 053202.
(19) Kawamata, H.; Negishi, Y.; Nakajima, A.; Kaya, K. *Chem. Phys. Lett.* **2001**, *337*, 255.
(20) Pramann, A.; Nakajima, A.; Kaya, K. *J. Chem. Phys.* **2001**, *115*, 5404.
(21) Kawamura, H.; Kumar, V.; Sun, Q.; Kawazoe, Y. *Phys. Rev. B* **2001**, *65*, 045406.
(22) Khanna, S. N.; Rao, B. K.; Jena, P. *Phys. Rev. B* **2002**, *65*, 125105.
(23) Dhavale, A.; Kanhere, D. G.; Blundell, S. A.; Zope, R. R. *Phys. Rev. B* **2002**, *65*, 085402.
(24) Boldyrev, A. I.; Wang, L. S. *J. Phys. Chem. A* **2001**, *105*, 10759.
(25) Li, X.; Wang, L. S.; Boldyrev, A. I.; Simons, J. *J. Am. Chem. Soc.* **1999**, *121*, 6033.
(26) Wang, L. S.; Boldyrev, A. I.; Li, X.; Simons, J. *J. Am. Chem. Soc.* **2000**, *122*, 7681.
(27) Boldyrev, A. I.; Simons, J.; Li, X.; Wang, L. S. *J. Chem. Phys.* **1999**, *111*, 4993.
(28) Li, X.; Zhang, H. F.; Wang, L. S.; Geske, G. D.; Boldyrev, A. I. *Angew. Chem., Int. Ed.* **2000**, *39*, 3630.
(29) Boldyrev, A. I.; Li, X.; Wang, L. S. *Angew. Chem., Int. Ed.* **2000**, *39*, 3307.

π-aromaticity)[30−33] have been discovered in small Al-based clusters. The all-metal aromatic clusters consist of X_4^{2-} units (X = group 13 elements), and they have been found in organogallium compounds as key structural units.[33,34] The isovalent and isosteric Hg_4^{6-} units existing in ancient amalgams have also been considered to possess similar aromatic characteristics.[35] However, the question remains if the X_4^{2-} aromatic units can be incorporated into "sandwich"-type complexes or if they would fuse together to form large clusters without ligand protections. More recently, two of the current authors reported theoretical evidence of both σ- and π-aromaticity in even smaller X_3^- species (X = B, Al, Ga).[36] It was also found that the structural and electronic integrity of the Al_3^- anion is maintained inside a $Na^+Al_3^-$ salt molecule, analogous to the $X_4^{2-}Na^+_2$ or $Hg_4^{6-}Na^+_6$ species. The Al_3^- anion is certainly among the smallest inorganic aromatic molecules possessing both π- and σ-aromaticity and provides an excellent opportunity to address the issue of what happens when two such aromatic units are brought together to form Al_6^{2-}.

However, as a doubly charged anion, Al_6^{2-} is expected to be unstable in the gas phase due to intracluster Coulomb repulsion. To prepare it experimentally, at least one counterion is required to stabilize it in the form of $M^+[Al_6^{2-}]$ (MAl_6^-), which would also be convenient for mass analyses and photodetachment experiments. In this article, we report a combined photoelectron spectroscopy (PES) and ab initio study on a series of MAl_6^- species (M = Li, Na, K, Cu, and Au). As we showed previously,[24−31] combining PES and ab initio calculations is a powerful means to obtain detailed information about the structure and bonding of novel gaseous clusters. In the current experiment, well-resolved PES data were obtained at three photon energies. The experimental results were compared with the ab initio calculations, allowing the structural and electronic properties of Al_6^{2-} and $M^+[Al_6^{2-}]$ to be well characterized. Furthermore, through detailed MO analyses, we were able to understand the structures and MOs of Al_6^{2-} in terms of the fusion of two Al_3^- units and explore three-dimensional π- and σ-aromaticity in MAl_6^- and Al_6^{2-}.

Experimental Method

The experiment was carried out using a magnetic-bottle time-of-flight PES apparatus equipped with a laser vaporization supersonic cluster source, the details of which have been described previously.[37,38] Briefly, the MAl_6^- (X = Li, Na, Cu, and Au) anions were produced by laser vaporization of appropriate aluminum-mixed targets in the presence of a helium carrier gas. The targets were made by compressing a mixture of either M_2CO_3 (M = Li and Na) compound powder or pure M (M = Cu and Au) powder with an aluminum powder at the appropriate molar ratios. Various clusters were produced from the cluster source for each target and were mass analyzed using a time-of-flight mass spectrometer. In each experiment, the MAl_6^- species was mass-selected and decelerated before being photodetached. Three detachment photon energies were used in the current experiment: 355 nm (3.496 eV), 266 nm (4.661 eV), and 193 nm (6.424 eV). Photoelectrons were collected at nearly 100% efficiency by the magnetic bottle and analyzed in a 3.5 m long electron flight tube. The photoelectron spectra were calibrated using the known spectrum of Rh^-, and the resolution of the apparatus was better than 30 meV for 1 eV electrons.

Computational Methods

We performed ab initio calculations on a wide variety of structures for Al_6^{2-} and MAl_6^- (M = Li, Na, K, and Cu) to search for the global minimum. We initially optimized geometries and calculated frequencies of Al_6^{2-} and MAl_6^- using analytical gradients with polarized split-valence basis sets (6-311+G*)[39−41] and a hybrid method known in the literature as B3LYP.[42−44] Two of the most stable structures of Al_6^{2-} and $LiAl_6^-$ were further optimized using the quadratic configuration interaction method [QCISD][45] with the 6-311+G* basis sets. The energies of the most stable structures were then refined using the coupled-cluster method [CCSD(T)][46−48] and the more extended 6-311+G(2df) basis sets. The vertical electron detachment energies (VDEs) for MAl_6^- (M = Li, Na, K, and Cu) were calculated using the outer valence Green Function method[49−53] [OVGF/6-311+G(2df)] and B3LYP/6-311+G* geometries. Core electrons were kept frozen in treating the electron correlation at the CCSD(T) and the OVGF levels of theory. All calculations were performed using the Gaussian 98 program.[54] Molecular orbitals for Al_3^-, Al_6^{2-}, $NaAl_6^-$, and $CuAl_6^-$ were calculated at the RHF/6-311+G* level of theory. All MO pictures were made using the MOLDEN 3.4 program.[55] $AuAl_6^-$ was not calculated in the present study due to the strong relativistic effects anticipated for Au. However, its structure is expected to be similar to that of $CuAl_6^-$, as is evident in their similar PES spectra (see below). KAl_6^- was included here to facilitate comparisons with previous theoretical studies, although it was expected to be similar to $LiAl_6^-$ and $NaAl_6^-$.

Experimental Results

The PES spectra of MAl_6^- (X = Li, Na, Cu, and Au) at three photon energies are shown in Figures 1 and 2. The observed electronic transitions are labeled with letters, and the vertical

(30) Li, X.; Kuznetsov, A. E.; Zhang, H. F.; Boldyrev, A. I.; Wang, L. S. *Science* **2001**, *291*, 859.
(31) Li, X.; Zhang, H. F.; Wang, L. S.; Kuznetsov, A. E.; Cannon, N. A.; Boldyrev, A. I. *Angew. Chem., Int. Ed.* **2001**, *40*, 1867.
(32) Boldyrev, A. I.; Kuznetsov, A. E. *Inorg. Chem.* **2002**, *41*, 532.
(33) Kuznetsov, A. E.; Boldyrev, A. I.; Li, X.; Wang, L. S. *J. Am. Chem. Soc.* **2001**, *123*, 8825.
(34) Twamley, B.; Power, P. P. *Angew. Chem., Int. Ed.* **2000**, *39*, 3500.
(35) Kuznetsov, A. E.; Corbett, J. D.; Wang, L. S.; Boldyrev, A. I. *Angew. Chem., Int. Ed.* **2001**, *40*, 3369.
(36) Kuznetsov, A. E.; Boldyrev, A. I. *Struct. Chem.* **2002**, *13*, 141.
(37) Wang, L. S.; Cheng, H. S.; Fan, J. *J. Chem. Phys.* **1995**, *102*, 9480.
(38) Wang, L. S.; Wu, H. In *Advances in Metal and Semiconductor Clusters. IV. Cluster Materials*; Duncan, M. A., Ed.; JAI Press: Greenwich, 1998; pp 299−343.
(39) McLean, A. D.; Chandler, G. S. *J. Chem. Phys.* **1980**, *72*, 5639.
(40) Clark, T.; Chandrasekhar, J.; Spitznagel, G. W.; Schleyer, P. v. R. *J. Comput. Chem.* **1983**, *4*, 294.
(41) Frisch, M. J.; Pople, J. A.; Binkley, J. S. *J. Chem. Phys.* **1984**, *80*, 3265.
(42) Parr, R. G.; Yang, W. *Density-Functional Theory of Atoms and Molecules*; Oxford University Press: Oxford, 1989.
(43) Becke, A. D. *J. Chem. Phys.* **1992**, *96*, 2155.
(44) Perdew, J. P.; Chevary, J. A.; Vosko, S. H.; Jackson, K. A.; Pederson, M. R.; Singh, D. J.; Fiolhais, C. *Phys. Rev. B* **1992**, *46*, 6671.
(45) Pople, J. A.; Head-Gordon, M.; Raghavachari, K. J. A. *J. Chem. Phys.* **1987**, *87*, 5958.
(46) Cizek, J. *Adv. Chem. Phys.* **1969**, *14*, 35.
(47) Purvis, G. D., III; Bartlett, R. J. *J. Chem. Phys.* **1982**, *76*, 1910.
(48) Scuseria, G. E.; Janssen, C. L.; Schaefer, H. F., III. *J. Chem. Phys.* **1988**, *89*, 7282.
(49) Cederbaum, L. S. *J. Phys. B* **1975**, *8*, 290.
(50) von Niessen, W.; Shirmer, J.; Cederbaum, L. S. *Comput. Phys. Rep.* **1984**, *1*, 57.
(51) Zakrzewski, V. G.; von Niessen, W. *J. Comput. Chem.* **1993**, *14*, 13.
(52) Zakrzewski, V. G.; Ortiz, J. V. *Int. J. Quantum Chem.* **1995**, *53*, 583.
(53) For a recent review, see: Ortiz, J. V.; Zakrzewski, V. G.; Dolgunitcheva, O. In *Conceptual Trends in Quantum Chemistry*; Kryachko, E. S., Ed.; Kluver: Dordrecht, 1997; Vol. 3, p 463.
(54) Frisch, M. J.; Trucks, G. W.; Schlegel, H. B.; Gill, P. M. W.; Johnson, B. G.; Robb, M. A.; Cheeseman, J. R.; Keith, T.; Petersson, G. A.; Montgomery, J. A.; Raghavachari, K.; Al-Laham, M. A.; Zakrzewski, V. G.; Ortiz, J. V.; Foresman, J. B.; Cioslowski, J.; Stefanov, B. B.; Nanayakkara, A.; Challacombe, M.; Peng, C. Y.; Ayala, P. Y.; Chen, W.; Wong, M. W.; Andres, J. L.; Replogle, E. S.; Gomperts, R.; Martin, R. L.; Fox, D. J.; Binkley, J. S.; Defrees, D. J.; Baker, J.; Stewart, J. P.; Head-Gordon, M.; Gonzalez, C.; Pople, J. A. *Gaussian 94*, revision A.1; Gaussian, Inc.: Pittsburgh, PA, 1995.
(55) The MO pictures were made using the MOLDEN3.4 program. Schaftenaar, G. *MOLDEN3.4*; CAOS/CAMM Center: The Netherlands, 1998.

Table 1. Observed Vertical and Adiabatic Detachment Energies (VDEs and ADEs) in eV, Vibrational Frequencies in cm^{-1}, and ab Initio VDEs in eV for MAl_6^- (M = Li, Na, K, Cu, and Au)

	C_{2v}		C_{3v}		obs	VDE	ADE	vib. freq
species	MO	VDE (theo)[a]	MO	VDE (theo)[a]	feature	(exp)[b]	(exp)[b]	(exp)[b]
$LiAl_6^-$	$5a_1$	2.39 (0.86) [2.39 (0.86)][c]	3e	2.47 (0.87)	X	2.55 (5)	2.43 (4)[d]	
	$2b_1$	2.42 (0.87) [2.41 (0.87)]						
	$4a_1$	2.81 (0.86) [2.83 (0.87)]	$4a_1$	2.55 (0.87)	A	2.70 (3)		
	$3a_1$	3.08 (0.86) [3.10 (0.86)]	$3a_1$	2.93 (0.87)	B	3.07 (2)	3.07 (2)	270 (50)
	$2b_2$	3.62 (0.85) [3.61 (0.86)]	2e	3.53 (0.86)	C	3.58 (4)	3.49 (5)	
	$1a_2$	3.67 (0.85) [3.63 (0.85)]						
$NaAl_6^-$	$5a_1$	2.22 (0.86)	3e	2.31 (0.86)	X	2.40 (5)	2.28 (4)[d]	
	$2b_1$	2.24 (0.86)						
	$4a_1$	2.69 (0.86)	$4a_1$	2.32 (0.87)	A	2.55 (8)		
	$3a_1$	2.94 (0.86)	$3a_1$	2.81 (0.87)	B	2.97 (3)	2.97 (3)	
	$2b_2$	3.42 (0.85)	2e	3.39 (0.86)	C	3.46 (5)	3.36 (5)	
	$1a_2$	3.63 (0.85)						
KAl_6^-	$5a_1$	1.89 (0.87)	$4a_1$	2.00 (0.87)				
	$2b_1$	2.01 (0.87)	3e	2.08 (0.87)				
	$4a_1$	2.52 (0.86)						
	$3a_1$	2.44 (0.88)	$3a_1$	2.59 (0.87)				
	$2b_2$	3.25 (0.85)	2e	3.16 (0.86)				
	$1a_2$	3.40 (0.85)						
$CuAl_6^-$	$3b_1$	2.74 (0.87)	5e	2.74 (0.87)	X	2.80−2.95[e]	2.77 (3)[d]	
	$7a_1$	2.89 (0.87)			A	2.80−2.95[e]		
	$6a_1$	3.04 (0.87)	$5a_1$	2.98 (0.87)	B	3.14 (2)	3.14 (2)	240 (50)
	$5a_1$	3.36 (0.87)	$4a_1$	3.29 (0.87)	C	3.55 (3)	3.46 (5)	
	$3b_2$	3.75 (0.86)	4e	3.81 (0.87)	C′	3.80 (3)	3.71 (4)	
	$2a_2$	3.80 (0.87)						
$AuAl_6^-$					X	2.83 (3)	2.83 (3)[d]	
					A	2.96 (3)	2.96 (3)	160 (40)
					B	3.19 (2)	3.19 (2)	320 (20)
					C	3.85 (6)	3.80 (6)	
					C′	3.97 (7)		

[a] The VDEs were calculated at the OVGF/6-311+G(2df)//B3LYP/6-311+G* level of theory. The numbers in the parentheses indicate the pole strength, which characterizes the validity of the one-electron detachment picture. The ground-state VDEs and ADEs evaluated at the B3LYP/6-311+G* level of theory are 2.45 and 2.22 eV (C_{3v}, $LiAl_6^-$); 2.35 and 2.27 eV (C_{2v}, $LiAl_6^-$); 2.32 and 2.08 eV (C_{3v}, $NaAl_6^-$); 2.27 and 2.21 eV (C_{2v}, $NaAl_6^-$); 1.98 and 1.93 eV (C_{3v}, KAl_6^-); 1.90 and 1.86 eV (C_{2v}, KAl_6^-); 2.88 and 2.82 eV (C_{3v}, $CuAl_6^-$); 2.81 and 2.67 eV (C_{2v}, $CuAl_6^-$), respectively. [b] The numbers in the parentheses represent the uncertainties in the last digits. [c] The VDEs in brackets were calculated at the OVGF/6-311+G(2df)//QCISD/6-311+G* level of theory. The numbers in the parentheses indicate the pole strength, which characterizes the validity of the one-electron detachment picture. [d] Adiabatic electron affinities of the corresponding neutral species. [e] Unresolved broad band.

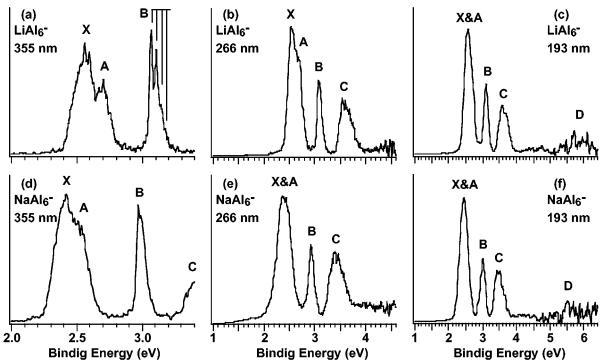

Figure 1. Photoelectron spectra of $LiAl_6^-$ and $NaAl_6^-$ at three photon energies: 355 nm (3.496 eV), 266 nm (4.661 eV), and 193 nm (6.424 eV).

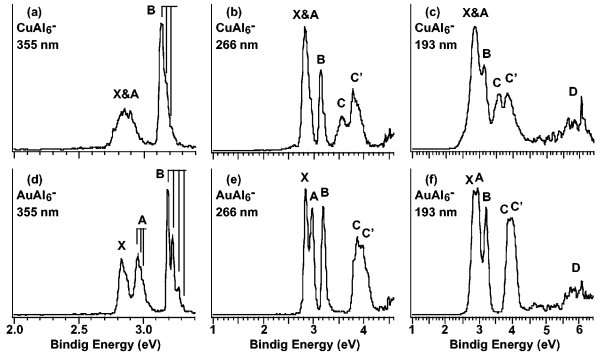

Figure 2. Photoelectron spectra of $CuAl_6^-$ and $AuAl_6^-$ at three photon energies.

lines in the 355 nm spectra represent resolved vibrational structures. All of the obtained electronic binding energies and vibrational frequencies are collected in Table 1, where they are compared with ab initio calculations.

$LiAl_6^-$. The 355 nm spectrum of $LiAl_6^-$ revealed a relatively broad ground-state transition X with a VDE of 2.55 eV (Figure 1a). This band contained discernible fine features, but they were not well resolved, probably due to the excitation of more than one vibrational mode upon photodetachment. Because no clean vibrational structures were observed for the ground-state transition, the adiabatic detachment energy (ADE) of $LiAl_6^-$ or the electron affinity (EA) of $LiAl_6$ was evaluated by drawing a straight line at the leading edge of the X band and adding a constant to the intersection with the binding energy axis to take into account the instrumental resolution. The relatively sharp onset of the X band defines a fairly accurate ADE of 2.43 eV for $LiAl_6^-$, which also represents the EA of the corresponding

neutral $LiAl_6$ species. Band A with a VDE of 2.70 eV also showed fine features (Figure 1a), which were also likely due to unresolved vibrational structures. This band has lower intensity relative to the X band. At the higher binding energy side of the 355 nm spectrum, a well-resolved vibrational progression (band B) with a spacing of 270 cm^{-1} was revealed. This band is the sharpest among all of the four main bands observed for $LiAl_6^-$, indicating only a small geometry change from the anion to the neutral upon detaching an electron from the corresponding MO. The 0−0 transition defines an ADE of 3.07 eV for the B band, which also represents the VDE.

An additional broad band C with a VDE of 3.58 eV and discernible fine features was observed at 266 nm (Figure 1b). The onset of the C feature is well-defined, from which an ADE of 3.49 eV was measured. The 193 nm spectrum did not reveal any intense new features. Yet some weak features (labeled as D) were observed at the higher binding energy side. These weak features were unlikely to be from one-electron transitions, but rather they may come from contributions of multielectron processes, as will be discussed below.

$NaAl_6^-$. The spectra of $NaAl_6^-$ (Figure 1d−f) are nearly identical to those of $LiAl_6^-$. Four main features (X, A, B, and C) were revealed for $NaAl_6^-$, as in $LiAl_6^-$. The ground-state feature X is again relatively broad, yielding an ADE of 2.28 eV and a VDE of 2.40 eV. Feature A with a VDE of about 2.55 eV is overlapped with band X and also exhibited a slightly lower intensity. Feature B, with a VDE and an ADE of 2.97 eV, was again the sharpest among all of the observed features similar to that of the $LiAl_6^-$ spectra. However, no well-resolved vibrational progression was observed for this band, in contrast to that of $LiAl_6^-$. We suspect that the vibrational spacing for this band is less than 200 cm^{-1}. Band C appeared as a high binding energy tail in the 355 nm spectrum, but it was well defined in the 266 and 193 nm spectra with a VDE of around 3.46 eV. The onset of the C feature, which is also relatively broad, defines an ADE of 3.36 eV. Weak features (labeled D) were again observed at the higher binding energy side for $NaAl_6^-$ in the 193 nm data, as in the spectrum of $LiAl_6^-$.

$CuAl_6^-$ and $AuAl_6^-$. The PES data for $CuAl_6^-$ and $AuAl_6^-$ are shown in Figure 2. These PES data exhibited some similarity in pattern to those for $LiAl_6^-$ and $NaAl_6^-$, but there are also marked differences. The X and A features of $CuAl_6^-$ were heavily overlapped, whereas in the spectra of $AuAl_6^-$ these two bands were well separated. In addition, the intensities of the X and A bands appeared to be similar, in contrast to those of $LiAl_6^-$ or $NaAl_6^-$, where the X band exhibited clearly higher intensity than the A band. We were able to estimate an ADE for the X band of $CuAl_6^-$ at 2.77 eV from the threshold. Yet we can only give a range of VDEs for both the X and the A bands as 2.80−2.95 eV (Table 1). The B band of $CuAl_6^-$ is again sharp with a partially resolved vibrational progression (average spacing 240 cm^{-1}) at 355 nm (Figure 2a). However, the C band was split into two well-separated features, labeled as C and C′ in Figure 2b and c. Weak features (D) at high binding energies were also observed in the 193 nm spectrum of $CuAl_6^-$, which were again similar to those of the alkali-Al_6^- data, but slightly stronger.

The 355 nm spectrum of $AuAl_6^-$ (Figure 2d) was most interesting. The X and A bands were well resolved each with discernible fine features due to vibrations. We were able to estimate a vibrational frequency for the A band (160 cm^{-1}). The B band of $AuAl_6^-$ gave a very well-resolved vibrational progression with a surprisingly large spacing of 320 cm^{-1}, the highest among the four MAl_6^- species. The C band of $AuAl_6^-$ also contained two discernible components (C′), which were not as well separated as that in the $CuAl_6^-$ spectra. The weak D features in the 193 nm spectrum of $AuAl_6^-$ were similar to those of $CuAl_6^-$.

The most striking spectral similarity among the four MAl_6^- species is the band B, which is almost identical in the spectra of the four species except for their different vibrational spacing, suggesting that the four species should have similar structures. The trend of the vibrational frequencies observed for band B along the MAl_6 series is as follows: $AuAl_6$ (320 cm^{-1}) > $LiAl_6$ (270 cm^{-1}) > $CuAl_6$ (240 cm^{-1}) > $NaAl_6$ (<200 cm^{-1}). This observation will be valuable to the understanding of the bonding trend along the MAl_6 series. All of the observed VDEs, ADEs, EAs, and vibrational frequencies for the $CuAl_6^-$ and $AuAl_6^-$ species are also collected in Table 1.

Theoretical Results

We found that the most stable structure for Al_6^{2-} is the O_h octahedron, as shown in Figure 3. The trigonal prism structure (D_{3h}) is a first-order saddle point on the intramolecular rearrangement potential energy surface. Addition of a cation to the Al_6^{2-} dianion yields two minima: a global minimum structure with the cation located on one face of the Al_6^{2-} octahedron (C_{3v}, $^1A_1$) and a local minimum with the cation coordinated to one of the square faces of the Al_6^{2-} trigonal prism (C_{2v}, $^1A_1$). Optimized B3LYP/6-311+G* geometries for the MAl_6^- ($M^+Al_6^{2-}$) (M = Li, Na, K, Cu) species are shown in Figure 3. Reoptimized geometries of the two lowest energy structures of Al_6^{2-} and $LiAl_6^-$ at QCISD/6-311+G* are very close to those at B3LYP/6-311+G*. The structure with the cation located on one of the triangular faces of the trigonal prism was found to be a saddle point. At the B3LYP/6-311+G* level of theory, the C_{3v} and C_{2v} structures are very close in energy. Yet at our highest CCSD(T)/6-311+G(2df) level of theory for all of the MAl_6^- (M = Li, Na, K, and Cu) species, we found that the C_{3v} ($^1A_1$) structure is the most stable with the C_{2v} ($^1A_1$) structure being 5.8−6.6 kcal/mol higher for M = Li, Na, K, and 4.3 kcal/mol higher for M = Cu, as given in Figure 3. Because these two structures have close energies, we calculated ab initio photoelectron spectra at the OVGF/6-311+G(2df) level of theory for both, as given in Table 1. Surprisingly, we found an excellent agreement between VDEs calculated at the OVGF/6-311+G(2df) and B3LYP/6-311+G* levels of theory. Only those VDEs accessible by the experiment are listed in Table 1; those beyond 6.5 eV are not listed. A total of six detachment channels were obtained for the C_{2v} structures, whereas only four were observed for the C_{3v} ground-state structures due to the degeneracy in two MOs (Table 1).

The ADEs represent the total energy differences between the ground states of the anions and the neutrals. Because it would be too expensive to calculate all of the neutral states, which are all open-shell (doublet states), at the CCSD(T)/6-311+G(2df) level of theory, we only calculated the ADEs at the B3LYP/6-311+G* levels of theory, as given in the footnote of Table 1. Alternatively, the ADEs can be evaluated computationally by subtracting an adiabatic correction calculated at the B3LYP/

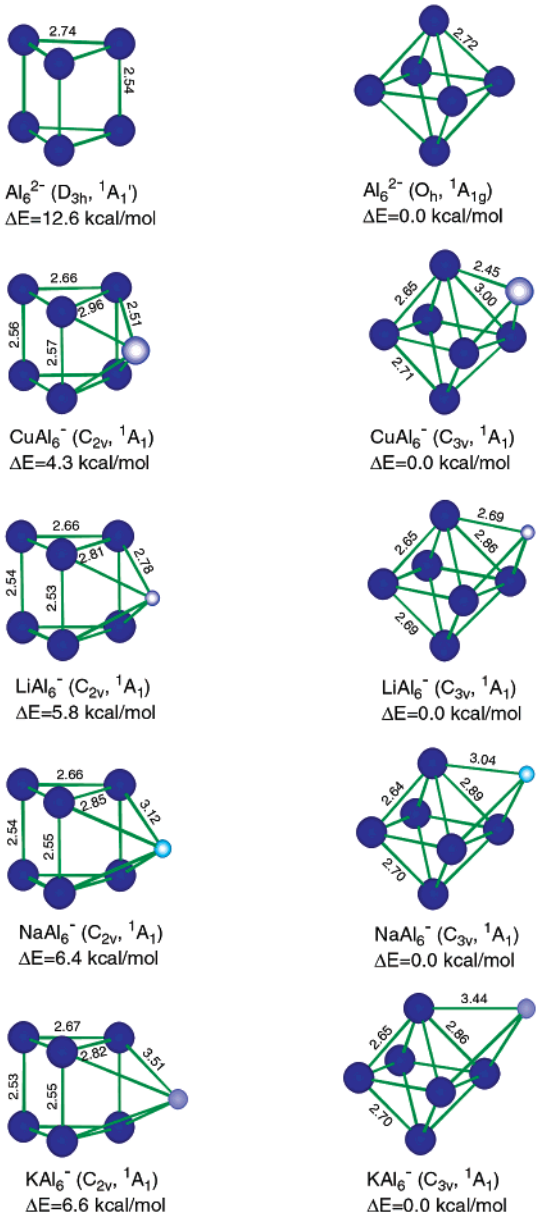

Figure 3. Optimized structures of Al_6^{2-} and MAl_6^- (M = Li, Na, K, and Cu) at the B3LYP/6-311+G* level of theory. The energies are calculated at the CCSD(T)/6-311+G(2df) level of theory.

6-311+G* level of theory from the VDEs calculated at the OVGF/6-311+G(2df) level of theory. By doing so we obtained a set of ADEs: 2.24 eV ($LiAl_6^-$, C_{3v}), 2.31 eV ($LiAl_6^-$, C_{2v}), 2.07 eV ($NaAl_6^-$, C_{3v}), 2.16 eV ($NaAl_6^-$, C_{2v}), 1.95 eV (KAl_6^-, C_{3v}), 2.18 eV (KAl_6^-, C_{2v}), 2.68 eV ($CuAl_6^-$, C_{3v}), and 2.60 eV ($CuAl_6^-$, C_{2v}). This set of values is consistent with those at the B3LYP/6-311+G* levels of theory, but should be slightly better.

Our prediction of the octahedral structure for the Al_6^{2-} dianion in the $LiAl_6^-$ and KAl_6^- clusters does not agree with a previous calculation using BPW91/LanL2DZ.[12] However, our obtained structure for $NaAl_6^-$ is consistent with a very recent DFT work on the same species.[23]

Interpretation of the Photoelectron Spectra

In addition to energetic information, ab initio calculations of VDEs using the OVGF method have been very helpful in the assignments and interpretation of experimental PES spectra.[24−31] This is particularly true for closed shell anions, which usually yield relatively simple PES spectra because there is a one-to-one correspondence between the occupied MOs and the observed spectra (barring strong Jahn−Teller or spin−orbit effects). Despite the relatively large size of the MAl_6^- clusters, they all yielded reasonably simple PES spectra, largely due to their closed shell nature. From our ab initio calculations, we found that the octahedron-Al_6-derived C_{3v} structures were the global minimum for all the MAl_6^- (M = Li, Na, K, and Cu) species, with the C_{2v} prism-derived structure as a low-lying isomer just a few kcal/mol higher in energy (Figure 3). The pole strengths, which are a measure of the validity of the single particle picture, for all of the calculated detachment channels for the two isomers (given in the parentheses in Table 1) are larger than 0.85, implying that the OVGF method is valid and all of the electron detachment channels can be considered as primarily one-electron processes.

Good agreement between the experimental and theoretical PES spectra is important for us to verify the ground-state structures of the anions. As we have shown previously,[24−31] the lowest energy structures always yield the best agreement with the experimental PES data. For the MAl_4^- ($M^+Al_4^{2-}$) clusters reported previously,[30] we found that both the alkali- and the coinage-metal-containing species have the same structures and bonding, although Cu^+ was observed to have much stronger interactions with the Al_4^{2-} unit. In the MAl_6^- clusters, we also observed similar PES spectra for the two systems (Figures 1 and 2), and our theoretical data for the two classes of MAl_6^- clusters are also similar (Figure 3). Again we observed considerably stronger interactions between Cu^+ and Al_6^{2-} than the alkali atoms, as reflected by the rather short Cu−Al bond lengths in both the C_{3v} and the C_{2v} isomers (Figure 3).

We found that the C_{3v} and C_{2v} isomers both gave similar PES data within the same binding energy ranges (Table 1). However, closer examination revealed that the ab initio VDEs of the C_{3v} isomers are in better agreement with the experimental data than those of the C_{2v} isomer. In particular, the ab initio VDE for the ground-state transition (X) of the C_{3v} isomer is in good agreement with the experimental VDE. The energy difference between the C_{2v} and C_{3v} species is sufficiently large (Figure 3), such that under the experimental conditions (room temperature) the C_{2v} isomers were not expected to be significantly populated. Therefore, in the following we will interpret the PES data on the basis of the C_{3v} ground-state structures.

Photoelectron Spectra of $LiAl_6^-$ and $NaAl_6^-$

The spectra of the two alkali-containing species are identical, and they both will be assigned and discussed together. The 10 valence MOs for $NaAl_6^-$ are shown in Figure 4. From our OVGF calculations, only detachments from the first six valence MOs were experimentally observed. The VDEs for the other four valence MOs are much higher and are outside the highest photon energy (6.424 eV) used in the current experiment.

Bands X and A. According to the ab initio calculations, the HOMO is the doubly degenerate 3e orbital (Figure 4). Detachment of a 3e electron from the C_{3v} MAl_6^- would give rise to a ^2E ground state for the neutral MAl_6 clusters, which would be expected to undergo Jahn−Teller distortion. The relatively broad feature for the X band is consistent with this assignment. Our

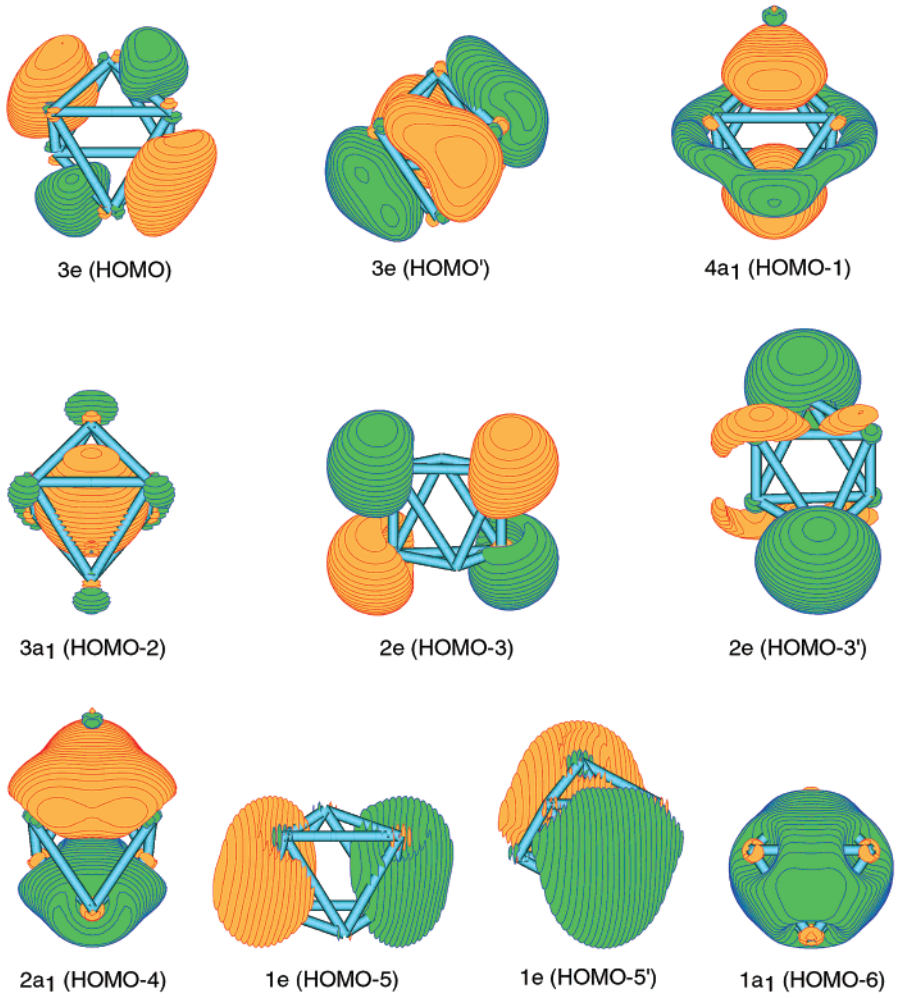

Figure 4. Molecular orbital pictures for the global minimum C_{3v} structure of $NaAl_6^-$.

calculated ADEs for $LiAl_6^-$ and $NaAl_6^-$ are 2.24 eV (C_{3v}) and 2.07 eV (C_{3v}), respectively, which are in reasonable agreement with the experimental values: 2.43 and 2.28 eV, respectively. Both the experimental and the theoretical VDEs are very close to the respective ADEs, suggesting that the structural distortions between the neutrals and anions are not very large. That is also in agreement with our computational results for the anionic and neutral species.

Detachment from HOMO-1 ($4a_1$) corresponds to the A band. The calculated VDE is very close to that of the 3e orbital for both $LiAl_6^-$ and $NaAl_6^-$, resulting in the overlapping and congested spectra for the X and A bands. The stronger spectral intensity for the X band relative to the A band is also consistent with the degeneracy of the corresponding MOs.

Band B. The B band is due to detachment of an electron from the $3a_1$ orbital (HOMO-2). This MO is highly unusual and has most of its electron density in the center of the Al_6^{2-} octahedron. It corresponds to the combination of the radial p orbital from each Al atom (Figure 4). The totally symmetric breathing mode involving the O_h Al_6^{2-} framework would be expected to be excited upon detachment from this MO. This is almost in perfect agreement with the experimental observation: the B band is the only band with a simple vibrational progression (Figure 1). Yet the vibrational spacing in the B band of $NaAl_6^-$ is too small for us to resolve a clean progression, but discernible vibrational features were observed (Figure 1d). Although the active mode should correspond to the totally symmetric breathing mode of the O_h Al_6 framework, it is clear that the alkali atom is significantly involved in this mode on the basis of the rather different vibrational spacing in the B bands of $LiAl_6^-$ and $NaAl_6^-$.

Band C. This band corresponds to detachment from the doubly degenerate 2e orbital (HOMO-3), which would again be expected to induce a Jahn−Teller effect upon photodetachment. This band is broad in the spectra of both $LiAl_6^-$ and $NaAl_6^-$, consistent with a possible Jahn−Teller effect.

Feature D. Our ab initio calculations suggested that there were no one-electron detachment channels between 4.5 and 7.7 eV for MAl_6^-. Although the OVGF method was not expected to be very reliable at the higher binding energy ranges (due to multielectron processes), this prediction was in qualitative agreement with our PES data, which showed that indeed there are no strong PES features beyond 4 eV in the 193 nm spectra (Figure 1). Thus, the very weak features (D) were likely due to multielectron transitions.

Photoelectron Spectra of $CuAl_6^-$ and $AuAl_6^-$

The valence MOs for the ground-state $CuAl_6^-$ species are shown in Figure 5. These MOs are very similar to those of $NaAl_6^-$ (Figure 4), except that the ordering is slightly different. The HOMO (5e) of $CuAl_6^-$ is again doubly degenerate, corresponding to the 3e HOMO of $NaAl_6^-$. The HOMO-1 ($5a_1$)

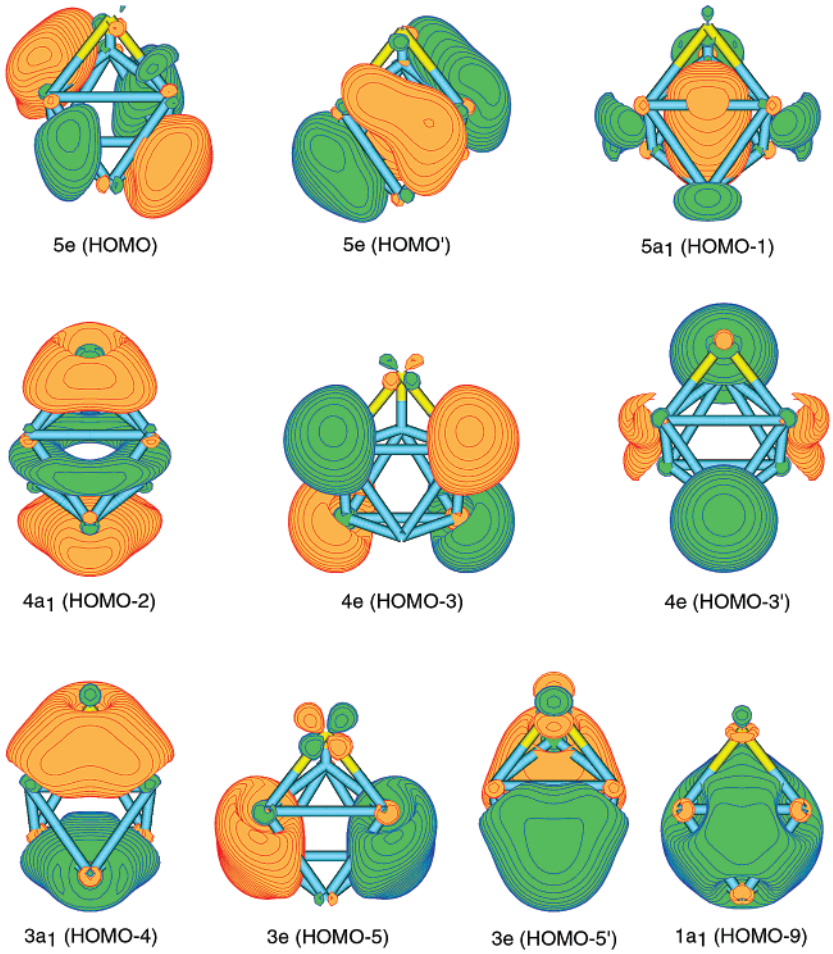

Figure 5. Molecular orbital pictures for the global minimum C_{3v} structure of $CuAl_6^-$.

of $CuAl_6^-$ corresponds to the HOMO-2 ($3a_1$) of $NaAl_6^-$, and the HOMO-2 ($4a_1$) of $CuAl_6^-$ corresponds to the HOMO-1 ($4a_1$) of $NaAl_6^-$. The ordering of all of the other MOs is identical in both systems. As we will see below, this difference in MO ordering between $NaAl_6^-$ and $CuAl_6^-$ is born out in the PES spectra. Although no calculations were performed on $AuAl_6^-$, the similarity of its PES spectra to those of $CuAl_6^-$ suggests that they should have similar structure and bonding and will be discussed together.

Bands X and A. These two heavily overlapped bands of $CuAl_6^-$ should correspond to the detachment of the doubly degenerate HOMO (5e), as a result of the Jahn−Teller splitting. Clearly the Jahn−Teller effect is stronger in $CuAl_6^-$ as compared to that in $NaAl_6^-$. It is even stronger in $AuAl_6^-$, resulting in two well-separated bands (Figure 2d). The detachment of the 3e HOMO of $LiAl_6^-$ or $NaAl_6^-$ only resulted in a broad band (X, Figure 1). Therefore, the labeled bands X and A in $CuAl_6^-$ are quite different from the labeled bands X and A in $LiAl_6^-$ or $NaAl_6^-$ because in the latter the A band represents a different detachment channel. This spectral assignment is in excellent agreement with the relative intensities of the X and A bands in the two systems.

Band B. This band is similar in all four MAl_6^- systems. It is the most outstanding feature in all of the PES spectra and provides almost a "fingerprint" for the four MAl_6^- species. In $CuAl_6^-$, it corresponds to detachment from the $5a_1$ orbital, which is the same MO that is responsible for the band B in $LiAl_6^-$ or $NaAl_6^-$. The consistency between this feature and the MO in all four systems provides the strongest support for our current assignments, verifying the obtained ground-state structures for these systems. As shown above for $NaAl_6^-$, the detachment from this unusual MO, which has most of its electron density in the center of the O_h Al_6^{2-} framework, should activate the totally symmetric breathing mode primarily of the Al_6^{2-} unit. As observed in the $LiAl_6^-$ and $NaAl_6^-$ species, the cation seems also to be significantly involved in this mode because the vibrational frequencies observed in the four systems are very different. The higher vibrational frequency observed in $CuAl_6^-$ suggests stronger interactions between Cu and Al, as is also reflected in the M−Al distances in Figure 3. The most surprising observation is the extremely high vibrational frequency (320 cm^{-1}) in the $AuAl_6^-$ system. This should be due to the strong relativistic effects anticipated for any clusters involving Au.

Bands C and C′. Band C should be due to detachment from HOMO-2 ($4a_1$). This MO corresponds to the $4a_1$ HOMO-1 in $NaAl_6^-$ (Figure 4), but it is considerably stabilized in $CuAl_6^-$. This can be understood by a more careful examination of the two MOs in $NaAl_6^-$ and $CuAl_6^-$. In $NaAl_6^-$ (Figure 4), the $4a_1$ MO represents an orbital with most of its electron density on the outside of the Al_6^{2-} framework. However, in $CuAl_6^-$ (Figure 5), the $4a_1$ orbital has significant density inside the Al_6^{2-} framework, representing a stronger bonding interaction between the top and bottom part of the Al_6^{2-} unit, leading to its considerable dropping in energy. This is also consistent with

the higher vibrational frequency observed for the Al_6^{2-} breathing mode in $CuAl_6$ than in $NaAl_6$.

The C′ band should be due to detachment of the 4e HOMO-3 (Figure 5). The broad feature of the C′ band is consistent with the degeneracy of the 4e orbital due to the Jahn−Teller effect. However, as compared to detachment from the 5e HOMO, the Jahn−Teller effect is small, particularly, in $AuAl_6^-$, where detachment of the 5e HOMO resulted in two well-separated bands (X and A), but the splitting from detachment of the 4e orbital is barely observable.

Feature D. For both isomers of $CuAl_6^-$, our ab initio calculations showed that there are no one-electron detachment channels between 4.5 and 7.7 eV, similar to the alkali-containing MAl_6^- species. The high binding energy features observed in the 193 nm spectra of $CuAl_6^-$ and $AuAl_6^-$ were similar to those observed in the spectra of $LiAl_6^-$ and $NaAl_6^-$, although they seemed to be more intense. Similarly, we assign these features to be due to multielectron transitions. Multielectron transitions are due to electron correlation effects. The stronger signals observed in the coinage-metal-containing species suggest that they have stronger electron correlation effects relative to the alkali-containing species.

Chemical Bonding in Al_6^{2-} and MAl_6^-

EA Trend. The EAs of the MAl_6 species are similar and span a narrow range from the lowest 2.28 eV for $NaAl_6$ to the highest 2.83 eV for $AuAl_6$ (Table 1). On the other hand, the EAs of the M atoms span a wide range: Na (0.55 eV) < Li (0.62 eV) < Cu (1.24 eV) < Au (2.31 eV).[56] The EA trends show that the HOMO of the MAl_6^- is derived mainly from Al, and hence the electronic structure of all MAl_6^- species resembles largely that of pure Al_6^{2-}. Otherwise, we may expect a large increase in EA from $LiAl_6$ to $CuAl_6$ to $AuAl_6$. This observation is born out from the MO analyses, as shown clearly in Figures 4 and 5. Despite the relatively strong interactions between Cu and Al, the valence MOs of $CuAl_6^-$ are largely dominated by the Al_6 framework, which can be effectively viewed as Al_6^{2-} interacting with Cu^+.

Relationship between the O_h Al_6^{2-} and D_{3h} Al_6^{2-}. Thus, the key to understanding the MAl_6^- species is to understand the bonding in Al_6^{2-}. As shown in Figure 3, the two lowest energy structures of MAl_6^- are derived from the O_h Al_6^{2-} and D_{3h} Al_6^{2-}. The latter is a saddle point 12.6 kcal/mol higher than the O_h global minimum. It is interesting to note that the Al−Al bond length (2.72 Å) in the O_h structure is very similar to the Al−Al bond length in the triangular face of the D_{3h} saddle point. Therefore, the D_{3h} structure can be viewed as a "transition state" between two O_h structures along an internal rotation of two Al_3^- units. The 12.6 kcal/mol energy represents a relatively small rotation barrier. In MAl_6^-, the D_{3h} Al_6^{2-} derived structures become local minima with much smaller energy differences from the O_h-derived ground states. Thus, it is conceivable that the barriers of the Al_3^- internal rotation would be even smaller in the MAl_6^- series.

Therefore, the structure and chemical bonding of the relatively complex Al_6^{2-} may be viewed effectively as the fusion of two Al_3^- units, which we previously showed is aromatic.[36] This fusion can be viewed as the stacking of two aromatic metal clusters, and it would be extremely interesting to understand how such fusion takes place at the molecular orbital level. This understanding will help us to learn about possible stacking of more aromatic Al_3^- units to form larger clusters, such as Al_9^{3-}, and ultimately about the possible formation of bulk solid materials. In the following, we first analyze the bonding and MOs of Al_3^-.[36]

Chemical Bonding and Aromaticity in Al_3^-. We previously showed that Al_3^- is doubly aromatic (σ and π) by comparing MOs of Al_3^- and $C_3H_3^+$.[36] The valence MOs of Al_3^- are shown in Figure 6a. The HOMO ($2a_1'$) of Al_3^- is formed from the in-plane Al 3p orbitals, and it is a σ-bonding MO. The HOMO-1 ($1a_2''$) is a π-bonding orbital formed from the out-of-plane 3p orbitals. The next three MOs ($1e'$ and $1a_1'$) are formed primarily from the filled valence Al 3s orbitals with rather small contributions from the Al 3p. When all bonding, nonbonding, and antibonding MOs composed of the same atomic orbitals (such as Al 3s in the current case) are occupied, the net bonding effect is expected to be close to zero, and the MOs can be viewed as lone pairs. The HOMO of $C_3H_3^+$ is a π-bonding orbital formed from the out-of-plane C 2p orbitals.[36] The next six MOs are linear combinations of hybridized sp^2 orbitals of C and 1s orbitals of H. These MOs can be transformed by some unitary transformation into three C−H σ-bonds and three C−C σ-bonds, thus giving rise to the classical description of the $C_3H_3^+$ cation.

The surprising result from the comparison of the MOs of Al_3^- with $C_3H_3^+$ is the earlier appearance of the π-MO ($1a_2''$) in Al_3^- before the pair of σ-MOs ($2e'$) is occupied (Figure 6a). The presence of the $1a_2''$ π-MO in Al_3^- is a violation of the canonical MO order observed in the $C_3H_3^+$ cation. What is even more surprising is that the π-MO is even lower in energy than the σ-bonding MO in Al_3^-. The presence of the delocalized π-MO ($1a_2''$) satisfies the $(4n + 2)$ aromaticity rule and renders π-aromaticity in Al_3^-. However, Al_3^- also has a delocalized σ-bond ($2a_1'$) (Figure 6a), and that renders σ-aromaticity in Al_3^-. Thus, the Al_3^- anion should be considered as being both σ- and π-aromatic.[36]

Chemical Bonding in O_h Al_6^{2-}: Fusion of Two Aromatic Al_3^- Units. Valence MOs of the global minimum O_h Al_6^{2-} are shown in Figure 6b. Comparing these MOs with those of $NaAl_6^-$ and $CuAl_6^-$ shows that they are rather similar except for differences in the ordering. One can see that the lowest six MOs ($1a_{1g}$, $1a_{2u}$, $1e_u$, and $1e_g$) of Al_6^{2-} are simply sums and differences between the three lowest MOs ($1a_1'$ and $1e'$) of Al_3^-, and thus they represent linear combinations of the six $3s^2$ lone pairs of Al. The next two MOs ($2a_{1g}$ and $3a_{1g}$) are sums of the delocalized σ ($2a_1'$) and π ($1a_2''$) MOs of Al_3^-, and they are responsible for bonding interactions between two Al_3^- units as well as within these groups. If, in Al_6^{2-}, the MOs corresponding to the differences between the $2a_1'$ and $1a_2''$ MOs of Al_3^- were also to be occupied (antibonding interactions between the two Al_3^- groups), the net bonding effect between the two Al_3^- units would be zero, and the formation of the octahedral Al_6^{2-} unit would not be possible. In such a case, one would have isolated Al_3^- units, for example, in a Na_2Al_6-type salt. However, instead of filling up antibonding orbitals, in Al_6^{2-} a sum of the lowest unoccupied MOs of Al_3^- are occupied, as schematically shown in Figure 7, providing additional bonding interactions between the Al_3^- groups. From this analysis, it is clear that the preferred

(56) Rienstra-Kiracofe, J. C.; Tschumper, G. S.; Schaefer, H. F., III; Nandi, S.; Ellison, G. B. *Chem. Rev.* **2002**, *102*, 231.

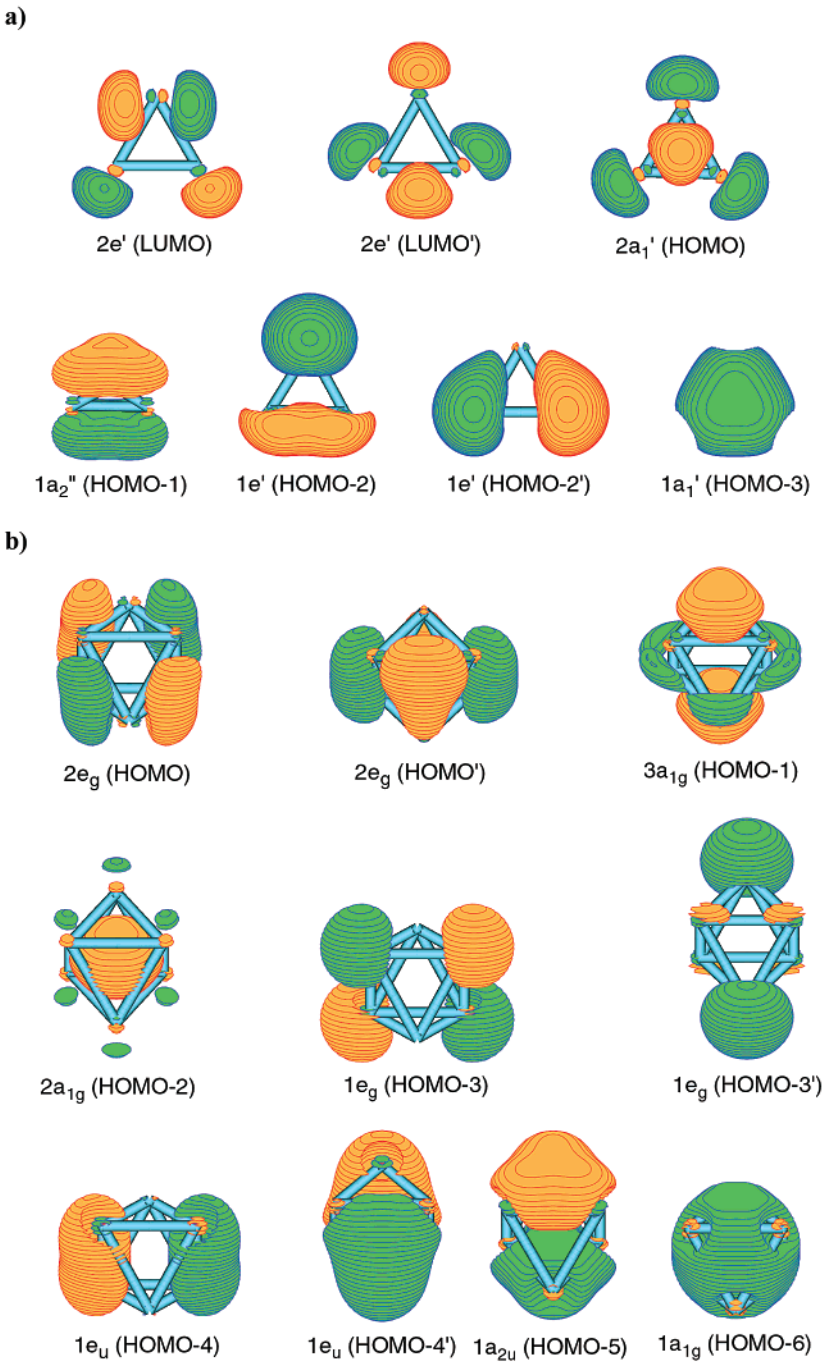

Figure 6. Molecular orbital pictures for (a) the aromatic Al_3^- (D_{3h}, $^1A_1'$) and (b) the global minimum structure of Al_6^{2-} (O_h, $^1A_{1g}$).

occupation of the bonding MOs derived from the 2e′ LUMOs of Al_3^- causes the fusion of two Al_3^- units into Al_6^{2-} and gives it structural stability.

Resonance Structures and Three-Dimensional Aromaticity in O_h Al_6^{2-}. The Al_6^{2-} dianion, just like Al_3^-, is electron deficient: there are only four bonding orbitals, but there are 12 Al−Al bonds in the O_h structure. Thus, chemical bonding in Al_6^{2-} should be represented through the use of a resonance of classical structures (with only two-center two-electron bonds). Let us first consider the resonance structures of Al_3^-, as shown in Figure 8a. Al_3^- has only two bonding orbitals, so the overall bond order for the three Al−Al bonds should be 0.66. In fact, the bond order should be considered 0.33 σ-bond and 0.33 π-bond because there is one σ- and one π-bond in Al_3^-, as shown in Figure 6a. A similar analysis for Al_6^{2-} reveals that there are 24 resonance structures, as illustrated in Figure 8b. Every resonance structure has one double bond and two single bonds. Averaging over the 24 structures gives us a bond order of 0.33, because there are 12 Al−Al bonds with only four bonding orbitals. These resonance structures provide an average octahedral structure with all six Al atoms being equivalent. Every resonance structure has three σ-bonds and one π-bond in agreement with the MO pictures in Figure 6b. Therefore, the 0.33 bond order can be split into 0.25 σ and 0.08 π. Thus, there is still both σ- and π-aromaticity on every face of the octahedron, that is, three-dimensional aromaticity.

Resonant Stabilization in Al_3^- and MAl_6^-. The presence of aromaticity in Al_3^- and Al_6^{2-} should manifest itself in

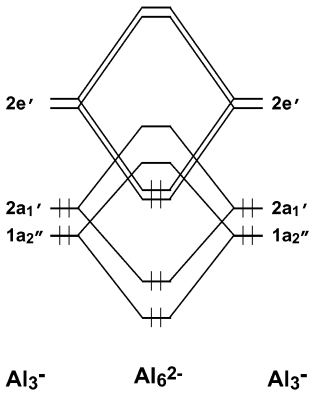

Figure 7. Schematic molecular orbitals showing the relationship between the valence orbitals of Al_6^{2-} and Al_3^-.

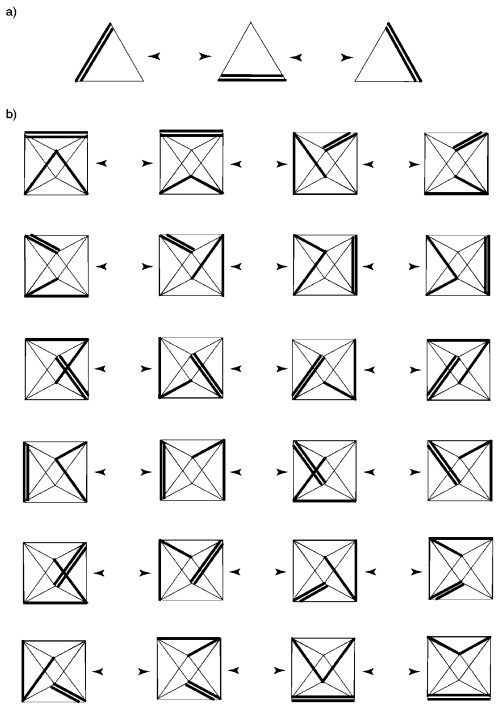

Figure 8. Resonance structures of (a) Al_3^- and (b) Al_6^{2-}.

additional stability to these species due to the resonance energy. The resonance energy in the current cases can be evaluated as a difference between the actual atomization energy and the atomization energy based on the resonance structure with classical two-center two-electron bonds. Because Al_6^{2-} is not an electronically stable entity, we use $NaAl_6^-$ to evaluate the resonance energies. We calculated the following dissociation energies for Al_3^- and $NaAl_6^-$ at the CCSD(T)/6-311+G(2df) level of theory:

$$Al_3^-(D_{3h}, {}^1A_1') \rightarrow 2Al(^2P) + Al^-(^3P) \qquad \Delta E = 120 \text{ kcal/mol} \quad (1)$$

$$NaAl_6^-(C_{3v}, {}^1A_1) \rightarrow 4Al(^2P) + Al^-(^3P) + NaAl(C_{\infty v}, {}^1\Sigma^+) \qquad \Delta E = 334 \text{ kcal/mol} \quad (2)$$

As one can see, the atomization energy (reaction 1) is unusually high for Al_3^-, clearly showing extra stability of the anion. To calculate the atomization energy of the classical structure, we need to evaluate the Al═Al double bond energy (see Figure 8a). We can evaluate an approximate value of the Al═Al double bond from the Al_2 diatomic molecule: D_0 = 32 kcal/mol [CCSD(T)/6-311+G(2df)][32] which is close to the experimental value of 31 kcal/mol.[57] The valence electronic configuration for Al_2 ($1\sigma_g^2 1\sigma_u^2 2\sigma_g^1 1\pi_u^1$)[57] shows that the first two MOs are bonding and antibonding orbitals composed from Al 3s orbitals, and the last two are σ-bonding ($2\sigma_g$) and π-bonding ($1\pi_u$) orbitals composed from the Al $2p_z$ and $2p_{x \text{ or } y}$ orbitals. Therefore, if both bonding orbitals are occupied by a single electron, the bond order in Al_2 ($^3\Pi_u$) can be approximately taken to be one (one-half from the σ-bond and one-half from the π-bond). If we double that (D_0 = 32 kcal/mol), we get an approximate value of 64 kcal/mol for the Al═Al double bond. We now can calculate the resonance energy as a difference of the energy of reaction 1 and the Al═Al double bond. It was found to be 56 kcal/mol, clearly showing the significant contributions from the σ- and π-aromaticity to the stability of Al_3^-.

The resonance energy in $NaAl_6^-$ is more difficult to estimate because of the presence of the sodium atom.[32] If we assume that the Na−Al bond energy in NaAl and the Na−Al bond energy in $NaAl_6^-$ are roughly the same, then we can evaluate the resonance energy in $NaAl_6^-$ by subtracting one Al═Al and two Al−Al bonds[32] (see resonance structures in Figure 8b) from the dissociation energy of reaction 2. The resonance energy calculated this way was found to be 216 kcal/mol. While this is a crude evaluation, it is certainly an extremely high value, and it will be very high regardless of the evaluation route one uses. This high value shows that the resonance energy increases with the degree of delocalization of the classical bonds. Thus, our resonance structure approach is able to explain why we have such high atomization energies in these aluminum clusters. More importantly, we are able to relate the bonding in the electron-deficient Al clusters to the classical two-center two-electron bond language, which has been so successful in organic chemistry.

Al_6^{2-} and the Violation of Wade's Rule. It should be pointed out that Wade's rules, which are usually used to explain structures of metal clusters in inorganic chemistry,[58,59] are not applicable to Al_6^{2-}. According to Wade's rules, the *closo*-deltahedra of n deltahedral atoms requires ($2n$ + 2) skeletal p-electrons. Thus, for an octahedron, Wade's rules require 14 skeletal p-electrons. The Al_6^{2-} dianion has only eight skeletal p-electrons, and therefore it should not be octahedral according to Wade's rules. We, therefore, believe that our interpretation of chemical bonding in Al_6^{2-} based on the concept of aromaticity and resonance is advantageous and that it may be applicable to a variety of metal clusters. We plan to explore this issue further in future works. It is hoped that advances of the aromaticity concept into metal clusters will help develop a unified view of chemical bonding in organic and inorganic chemistry.

Conclusions

A combined photoelectron spectroscopic and ab initio study is performed on a series of MAl_6^- (M = Li, Na, K, Cu, and Au) clusters. Well-resolved PES spectra were obtained for MAl_6^- (M = Li, Na, Cu, and Au) at three photon energies (355,

(57) Fu, Z.; Lemire, G. W.; Bishea, G. A.; Morse, M. D. *J. Chem. Phys.* **1990**, *90*, 8420.
(58) Wade, K. *Adv. Inorg. Chem. Radiochem.* **1976**, *18*, 1.
(59) Corbett, J. D. *Angew. Chem., Int. Ed.* **2000**, *39*, 670.

266, and 193 nm), yielding both vibrational and electronic information about the MAl_6 clusters. Ab initio energetics reveal that Al_6^{2-} possesses an octahedral O_h structure as the ground state. All of the MAl_6^- (M = Li, Na, K, and Cu) species possess a C_{3v} ground-state structure derived from the O_h Al_6^{2-}, with a C_{2v} isomer only a few kcal/mol higher in energy. Careful comparison between the PES spectra and the ab initio one-electron detachment energies allows us to establish firmly that the C_{3v} structures are the ground state for the MAl_6^- species. A detailed MO analysis is conducted for the O_h Al_6^{2-} and the C_{3v} $NaAl_6^-$. We found that Al_6^{2-} can be viewed as the fusion of two aromatic Al_3^- units. In Al_6^{2-}, the preferred occupation of MOs derived from the sums of the 2e′ LUMO of Al_3^-, rather than those derived from the differences between the $2a_1'$ and $2a_2''$ MOs of Al_3^-, provides the critical bonding interactions in Al_6^{2-}. It is these bonding HOMOs ($2e_g$) that cause the fusion of two aromatic Al_3^- units into the Al_6^{2-} species. We further found that every face of the Al_6^{2-} octahedron still possesses both π- and σ-aromaticity, analogous to the triangular Al_3^-, thus rendering three-dimensional π- and σ-aromaticity for Al_6^{2-} and MAl_6^-.

Acknowledgment. The theoretical work done at Utah was supported by the donors of the Petroleum Research Fund (ACS-PRF# 35255-AC6), administered by the American Chemical Society. The experimental work done at Washington was supported by the National Science Foundation (DMR-0095828) and was performed at the W. R. Wiley Environmental Molecular Sciences Laboratory, a national scientific user facility sponsored by DOE's Office of Biological and Environmental Research and located at Pacific Northwest National Laboratory, which is operated for DOE by Battelle.

JA027423G